Available online at www.sciencedirect.com

SCIENCE DIRECT®

Tectonophysics 401 (2005) 1–22

TECTONOPHYSICS

www.elsevier.com/locate/tecto

The Dudley earthquake of 2002: A moderate sized earthquake in the UK

Brian Baptie*, Lars Ottemoller, Susanne Sargeant, Glenn Ford, Aoife O'Mongain

British Geological Survey, Murchison House, West Mains Road, Edinburgh, UK

Received 21 June 2004; received in revised form 15 December 2004; accepted 21 February 2005
Available online 19 April 2005

Abstract

The 4.7 ML Dudley earthquake on 22 September 2002 at 23:53 (UTC) was widely felt throughout England and Wales, and was the largest earthquake to occur onshore in the United Kingdom (UK) since the magnitude 5.1 ML Bishop's Castle earthquake in 1990. The earthquake hypocentre, determined from inversion of observed *P*- and *S*-wave travel-time data, suggests a source depth of 14 km and this depth estimate is supported by forward modelling of observed waveforms. Focal mechanisms obtained from both first motion polarities of local observations and moment tensor inversion of regional observations show left-lateral, strike-slip faulting along a near vertical, near north–south striking fault plane whose orientation is in good agreement with the surface expression of the observed faults in the region. Two aftershocks were recorded within the location error ellipsoid of the mainshock. Comparison of the waveform signals revealed that the mainshock and aftershocks were nearly co-located and possibly had the same source mechanism. The observed peak ground acceleration is found to be less than that predicted using empirical relations, which have been considered applicable in the UK. Seismic moment M_0 and stress drop $\Delta\sigma$ were measured from on-scale records where L_g arrivals were clear, and then used to give better estimates of the peak ground accelerations using a stochastic approach.

Keywords: Earthquake; Source mechanism; Aftershocks; Faulting; Peak ground motion

1. Introduction

The Dudley earthquake on 22 September 2002 at 23:53 (UTC) was widely felt throughout England and Wales, and was the largest earthquake to occur onshore in the United Kingdom (UK) since the magnitude 5.1 ML Bishop's Castle earthquake in 1990 (Ritchie et al., 1990). The epicentre was about 3 km northwest of the town of Dudley in the West Midlands. A local magnitude was determined from amplitude readings at seismograph stations in the distance range 80 to 230 km and at a range of azimuths. The average magnitude based on readings from 9 stations was 4.7 ML. The UK is a country of low to moderate seismicity and the spatial distribution of earthquakes is generally diffuse, in keeping with

* Corresponding author. Tel.: +44 131 6500222; fax: +44 131 6671877.
E-mail address: b.baptie@bgs.ac.uk (B. Baptie).

0040-1951/$ - see front matter © 2005 Published by Elsevier B.V.
doi:10.1016/j.tecto.2005.02.010

other intra-plate areas. Main et al. (1999) suggest a maximum magnitude for UK earthquakes in the range 6.3–7.5 ML based on the observed Gutenberg–Richter frequency–magnitude law. By comparison, the largest so far observed is the magnitude 6.1 ML Dogger Bank earthquake of 1931 (Neilson et al., 1931). The recurrence relationship found by Musson (1994), based on the historical and instrumental earthquake catalogue for the UK, suggests that, on average, earthquakes of magnitude 4.7 ML, or greater, occur somewhere in the UK once in every 10 years. Events of comparable magnitude include the Carlisle earthquake in 1979, the Skipton earthquake in 1944 (Burton et al., 1984), the North Wales earthquake in 1940 (Musson et al., 1984) and the Caernarvon earthquake in 1903 (Musson et al., 1984). Fig. 1 shows the instrumental and historical seismicity of the West Midlands from 1768 to the present, in a 100 km^2 centred on the 2002 epicentre. Prior to 1970, the historical earthquake catalogue is expected to be reasonably complete for earthquakes greater than magnitude 4.0 ML. The seismicity in this region is generally diffuse, although, to the north and east of the 2002 epicentre, the seismicity follows a roughly north–northwest trend through Stafford. The largest earthquake in this area in the last hundred years was the 15 August 1926, 4.8 ML, event near Ludlow, which caused some minor damage, mostly to chimneys in the epicentral area. More recently, a magnitude 4.2 ML earthquake occurred near Warwick on 23 September 2000.

The earthquake was recorded throughout the UK, at seismograph stations operated by BGS (Simpson, 2002), and also regionally on broadband instrumentation operated by other agencies on mainland Europe. Fig. 2 shows the locations of seismograph

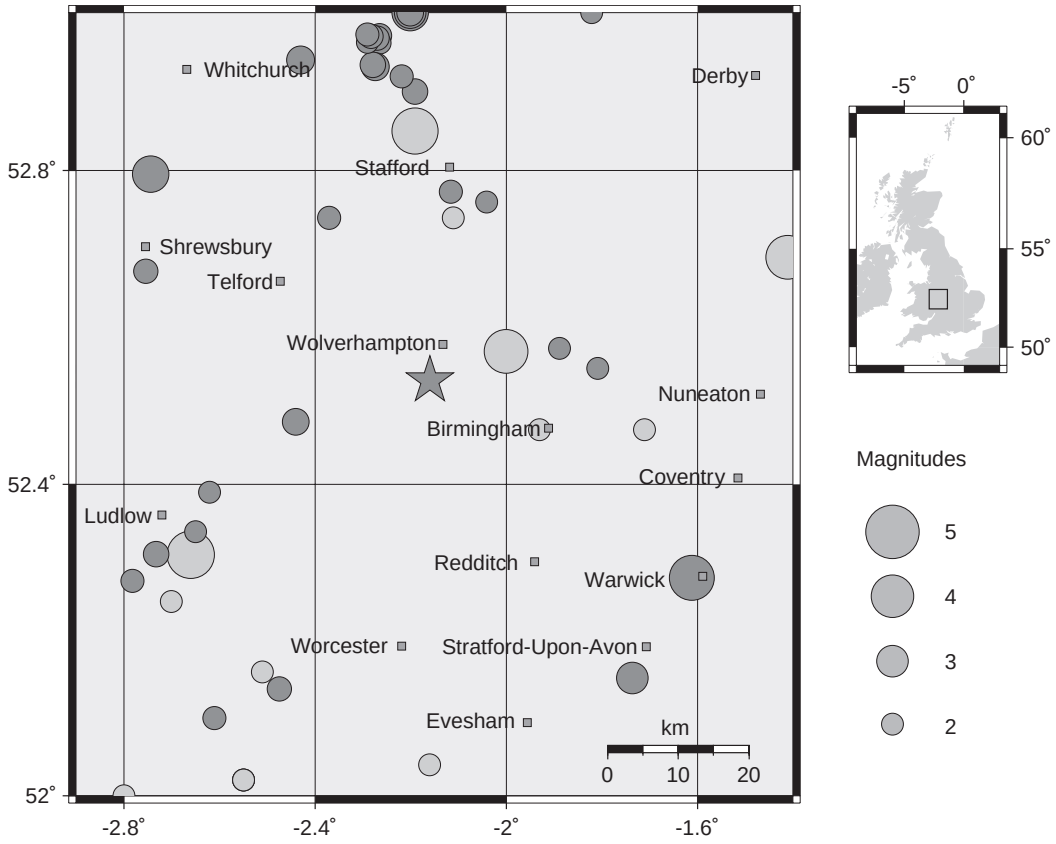

Fig. 1. Instrumental (dark circles) and historical (light circles) seismicity of the West Midlands from 1768 to the present, in a 100 km^2 centred on the 2002 epicentre, marked by the star.

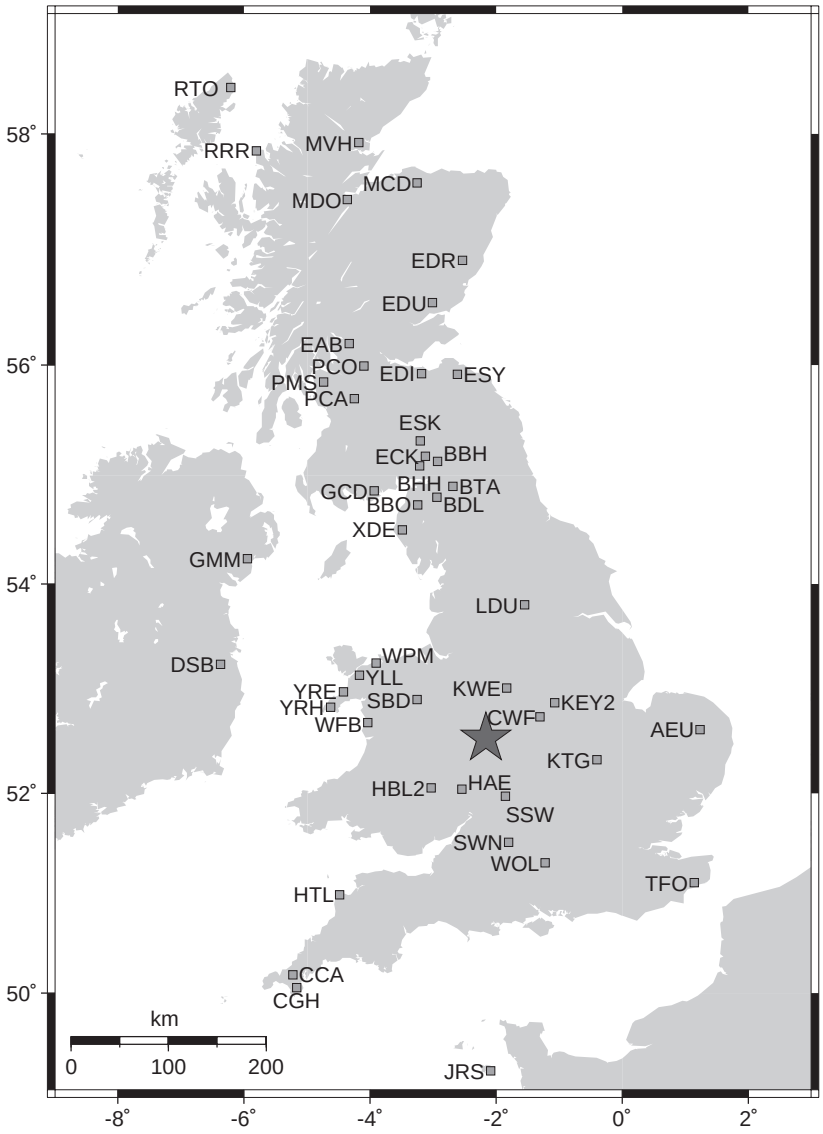

Fig. 2. Seismograph stations used in subsequent analyses. The 2002 epicentre is marked by a star.

stations used in subsequent analyses and mentioned specifically in the text. Much of the data recorded on the high-gain instrumentation operated by BGS was saturated. However, recordings made on lower gain instrumentation allowed accurate analysis of waveforms at a number of stations. Regional broad-band waveforms were used by researchers at the Swiss Seismological Service to determine a moment tensor solution for the source mechanism using full waveform modelling (Nabelek and Xia, 1995). The event was also observed at teleseismic distances on the Eilson seismic array, Alaska (ILAR) and the Makanchi seismic array, Kazakhstan (MKAR). Observations from the BGS network on mainland UK and Northern Ireland have been supplemented by data from seismograph stations operated by Keele University, the Atomic Weapons Establishment (AWE) at Blacknest and also IRIS. Two aftershocks were recorded, the first on 23 September at 03:32 (2.7 ML) about 3.5 h after the mainshock and the

second on 24 September at 09:29 (1.2 ML), some 30 h later.

The UK lies on the northwest European shelf and at the northeast margin of the North Atlantic Ocean. Its continental crust formed over a long period of time and has a complex tectonic history, with multiple episodes of deformation resulting in extensive faulting. No British earthquake recorded either historically or instrumentally has produced a surface rupture and typical fault dimensions for UK earthquakes are of the order of 1–2 km. Therefore, given the large uncertainties involved, it is difficult to associate earthquakes with specific faults, particularly at depth, where the fault distributions and orientations are unclear.

In this work, we present location and source parameters determined using common observatory practice for the Dudley mainshock and aftershocks. These results are discussed in the context of the tectonic setting and observed surface faulting. Waveform modelling of high-frequency near-source recordings is used to examine the depth constraint of the earthquake hypocentre. In addition, we examine the decay of peak ground acceleration with distance and compare this to the peak ground acceleration given by attenuation laws that are considered applicable to the UK. We then use random vibration theory to model peak horizontal ground acceleration (PHGA) as a function of distance for the mainshock and largest aftershock, using the seismic moment and Brune stress drop parameter determined from corrected displacement spectra. A first approximation of peak horizontal ground acceleration (PHGA) in the near-field is also made.

2. Geological setting

A wedge-shaped basement block of Proterozoic crust called the Midlands Microcraton dominates much of southern Britain (Pharaoh et al., 1993), and is bounded by the Variscan Front to the south and Welsh Caledonides to the North. The geological background of the West Midlands is summarised by Powell et al. (1992). A wide variety of sedimentary rocks were deposited over the time period between 430 and 225 Ma ago, and then subjected to folding, uplift and erosion several times following the Caledonian Orogeny, approximately 380 Ma ago. The final deformation phase (in the Permian) resulted in the Triassic sedimentary strata to the west and east of the Western and Eastern Boundary faults, respectively, being downthrown, defining the West Midlands Coalfield (Fig. 3). These faults are two of the numerous normal and reverse faults in the region, many of which dip steeply at the surface. More recently, periods of glaciation and intensive industrial development since the 18th century have had a significant effect on the near-surface geology of the West Midlands. Mineral deposits of coal, dolerite and limestone have been exploited extensively. As a result, there are significant areas of made ground. Dudley, Sedgely and Walsall are built above many small limestone quarries and larger sub-surface caverns, which are either open or partially back-filled.

3. Earthquake location

The Dudley earthquake was located using local recordings from available seismograph stations. *P*-wave arrivals were picked on vertical-component seismometers and *S*-wave arrivals on three-component seismometers where possible. Individual phases were assigned weightings based on a confidence level in the observed data, and the weighted arrival time data were input to the HYPOCENTER location algorithm (Lienert et al., 1988) to determine the earthquake hypocentre. In the absence of any definitive crustal velocity model for this area, from refraction or other sources, we used the 1-D velocity model shown in Table 1, determined from the LISPB refraction experiment (Bamford et al., 1978; Assumpção and Bamford, 1978), over northern Britain. Strictly speaking, this model is valid only for the Midland valley region of Scotland and contains a near-surface low-velocity zone; however, the model has been widely used to locate earthquakes throughout England and has given reasonable results. An additional weighting factor based on the distance parameters *xnear* and *xfar*, where the weight is linearly decreased from 1 to 0 between *xnear* and *xfar*, was used to systematically reduce weighting with distance and is typically applied to reduce the effect of lateral heterogeneity in the velocity model. In this case, an *xnear* of value 100 km and an *xfar* value of 300 km were applied. A total of 54 phase readings were used to determine the

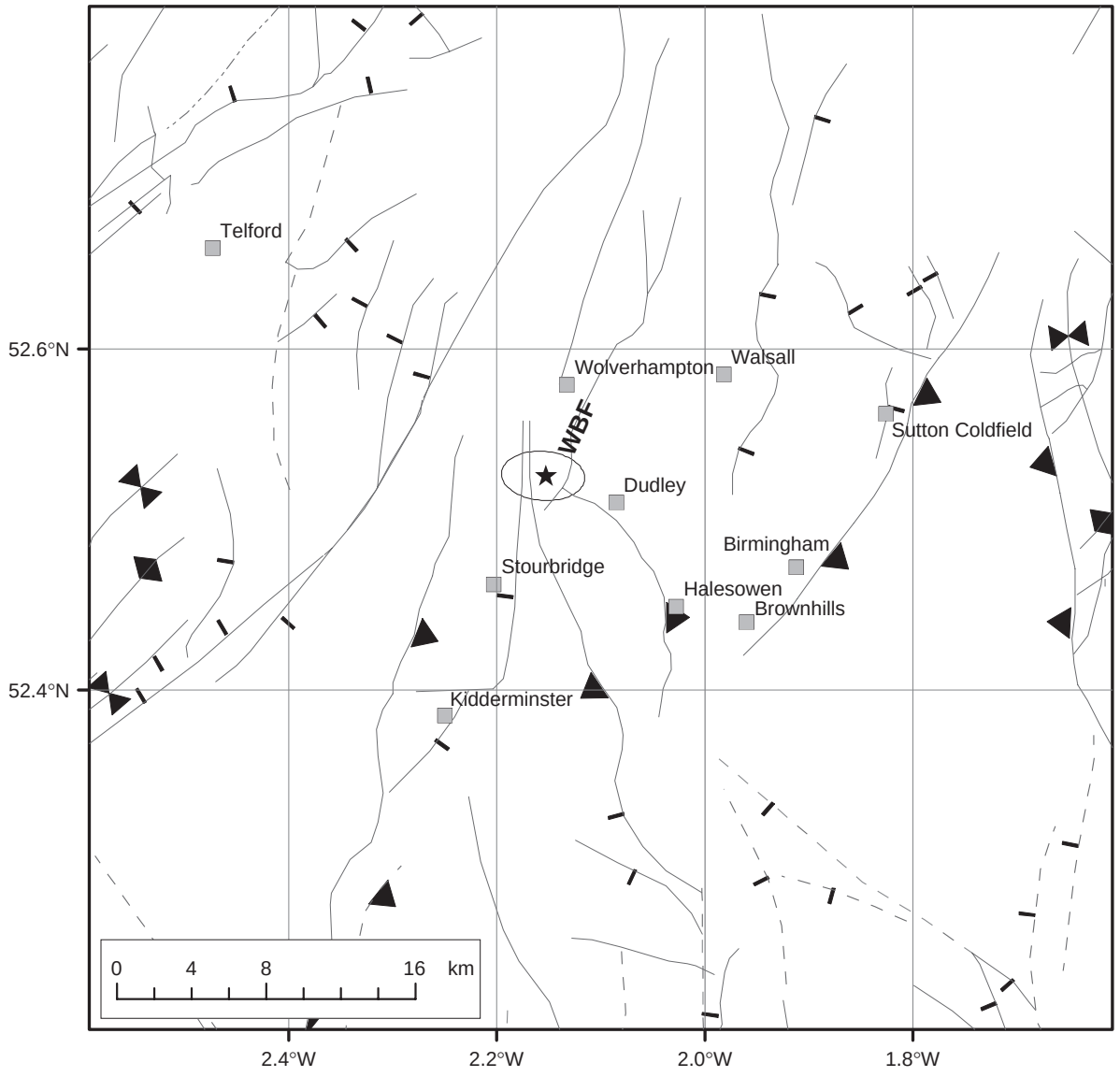

Fig. 3. Horizontal projection of the 90% confidence ellipsoid for the calculated hypocentre of the Dudley earthquake (marked by the star), along with surface trends of the principal faults in the West Midlands. Normal faults are denoted by a square on the downthrown side, while reverse faults are denoted by a barb on the upthrown side. The Western Boundary Fault is denoted by WBF.

earthquake hypocentre, giving an epicentre location of 52.526°N and 2.153°W, about 3 km northwest of Dudley, with horizontal errors of 1.6 km and 2.6 km in the north–south and east–west directions, respectively. Fig. 3 shows the horizontal projection of the 90% confidence ellipsoid for the calculated hypocentre. The overall RMS error in the hypocentral estimate is 0.33 s and the maximum azimuthal gap is 34°. Fig. 4 shows reduced *P*-wave travel-times for the Dudley earthquake as a function of epicentral distance for both observed (black circles) and modelled data. The theoretical *P*-wave travel-times for the primary crustal phases are determined for the 1-D velocity model used to locate the earthquake and a source depth of 14 km. The travel-time curves provide a reasonable match to the observed data, with the

Table 1
Crustal velocity model used in earthquake location

Depth to top of layer (km)	*P*-wave velocity (km/s)	V_p/V_s
0.00	4.00	1.73
2.52	5.90	1.73
7.55	6.45	1.73
18.87	7.00	1.73
34.15	8.00	1.73

modelled P_n phase providing a good fit to the data to epicentral distances of about 250 km.

The source depth was determined at 12.9 km with a corresponding error of 3.7 km. However, the nearest seismograph station to the epicentre is 58 km to the north–northeast and the nearest three-component seismograph station that recorded unsaturated *P*-wave and *S*-wave arrivals was 80 km to the southwest. In addition, considering the uncertainties associated with the 1-D velocity model, we expect the hypocentral depth to be poorly constrained. To further examine the depth resolution, we determined RMS error as a function of depth in the 0 to 30 km range with a spacing of 1 km. The results are shown in Fig. 5 and display a well-defined minimum at 14 km, suggesting that the assumption that the earthquake occurred at mid-crustal depths is reasonable.

4. Source mechanism

A source mechanism for the earthquake was determined using two different methods: we calculated a focal mechanism based on first motion polarities from locally recorded data within the UK;

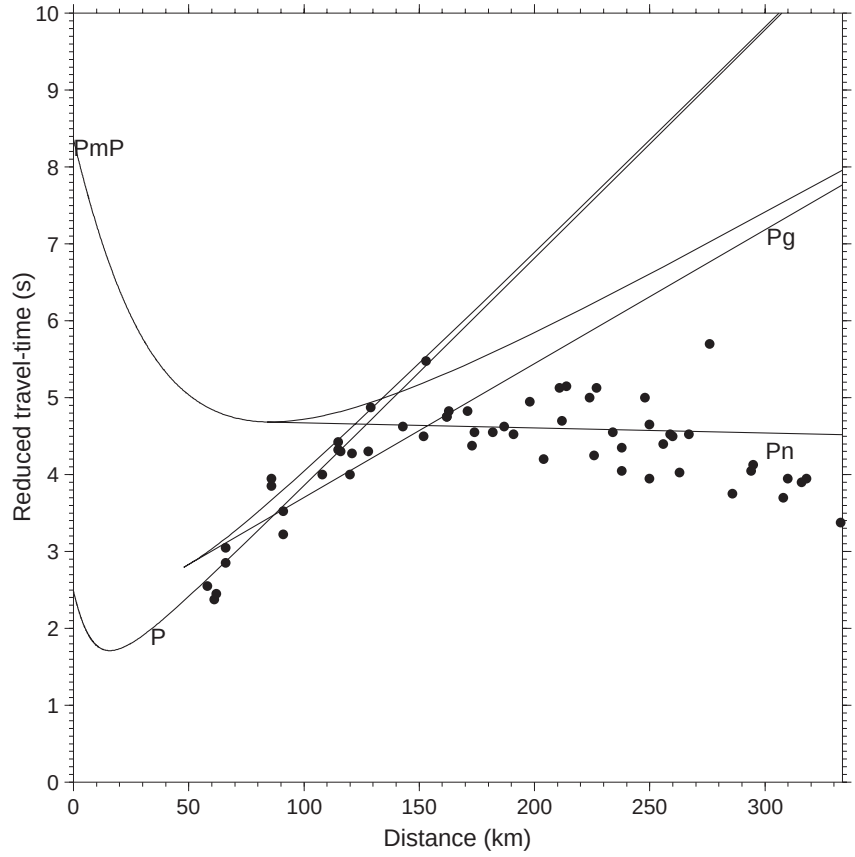

Fig. 4. Reduced *P*-wave travel times for the Dudley earthquake as a function of epicentral distance for both observed (black circles) and modelled data. Theoretical *P*-wave travel-time curves for primary crustal phases are determined for the 1-D velocity model used to locate the earthquake and a source depth of 14 km. The data have been reduced using a reduction velocity of 8 km/s.

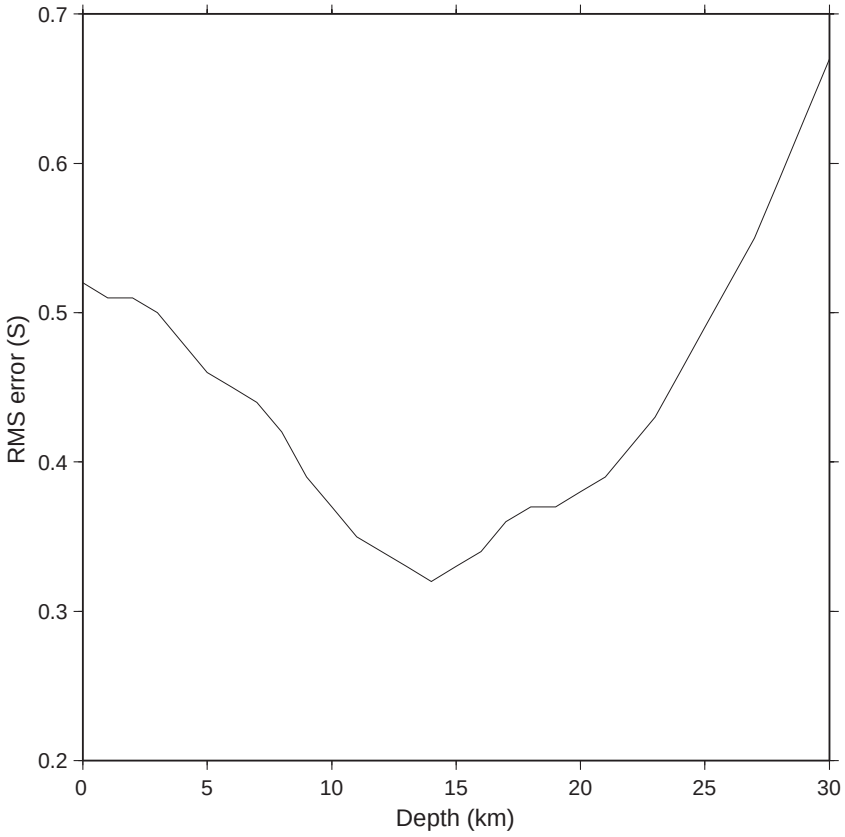

Fig. 5. RMS error in earthquake location as a function of depth.

secondly, the Swiss Seismological Service (SSS) determined a moment tensor solution based on waveform inversion of regional broadband recordings in the UK and other European countries (Bernardi et al., 2002). The regional moment tensor analysis of the SSS provides a source solution that explains the observed seismograms for long-period waves with minimal error (Nabelek and Xia, 1995). For the first-motion method, 57 *P*-wave polarities were picked from vertical component recordings at local seismograph stations at a wide range of azimuths. The grid search method of Snoke et al. (1984) was then used to determine the best-fitting fault plane solutions, with a grid spacing of 2°. The 1-D velocity model and a fixed source depth of 14 km were used to determine takeoff angles. Thirty-four possible solutions were found to fit the observed polarity data, which all showed very similar fault motion. The source mechanisms given by the two different methods are shown in Fig. 6. Both methods show near-vertical strike slip faults striking either north–south or east–west. The first motion data show either left-lateral strike-slip motion on a near-vertical north–south fault, dipping slightly to the east or right-lateral strike-slip motion on an east–west fault that could dip either north or south. The moment tensor solution shows either left-lateral strike-slip motion on a north–south fault, dipping to the west or right-lateral strike-slip motion on an east–west fault dipping to the south. We choose a solution from the first motion data that is most consistent with the moment tensor inversion with strike $\phi_s = 9^\circ$, dip $\delta = 86^\circ$ and rake $\lambda = -2^\circ$. The best fitting double couple from the moment tensor inversion has the parameters $\phi_s = 191^\circ$, $\delta = 82^\circ$ and $\lambda = 14^\circ$. The *P*-axis orientations given by the two methods are the same, with a *P*-axis azimuth and plunge of 324° and 4°, respectively. These directions agree well with the regional tectonic model, which predicts northwest

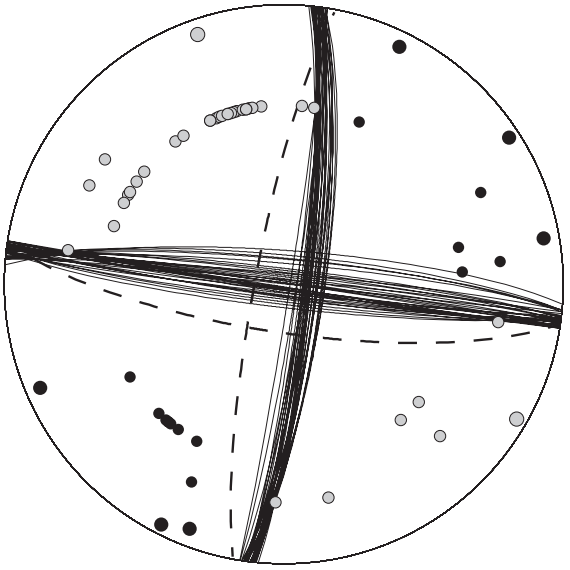

Fig. 6. Source mechanisms determined for the Dudley earthquake using first motion polarities from local recordings. The best-fitting double-couple solution given by moment tensor inversion of regional broadband waveforms obtained by the Swiss Seismological Service is shown by the dashed lines.

compression due to the opening of the mid-Atlantic ridge and also with a best-fitting stress tensor obtained by Baptie (2002) from inversion of fault plane solutions for UK earthquakes. The *T*-axis orientations are 180° apart, reflecting the difference in dip.

5. Waveform modelling

Given the source mechanism discussed above and the 1-D velocity model used for earthquake location, we applied the discrete wave number method of Herrmann (1996) to generate synthetic seismograms at different azimuths and epicentral distances for a number of fixed source depths. Fig. 7 shows observed and modelled ground displacement seismograms in a short time window about the initial *P*-wave arrival for four source depths of 12, 14, 16 and 18 km at four stations in the distance range 80–230 km. Visual comparison of the observed and modelled data shows that the models accurately capture many of the key characteristics of the observed data. For example, the synthetic seismograms for station WOL, Fig. 7(c), with source depth 14 km, shows the initial low amplitude *Pn* arrival followed by two higher amplitude phases (*PmP* and *Pg*), similar to those observed. Similarly, the 14 km source depth model at station AEU, Fig. 7(d), shows a low amplitude *Pn* followed by higher amplitude *PmP* and *Pg*, also observed in the data. The best match for the observed data at stations KEY2, Fig. 7(b), is also given by source depth of 14 km. However, the observed *P*-wave arrival at station HBL2, Fig. 7(a), is rather more complex than those modelled, with perhaps the 12 km source depth giving the best match. This highlights the degree of non-uniqueness in modelling high-frequency waveforms in the presence of uncertainties in the velocity model.

Fig. 8 shows observed and modelled seismograms for four stations in the 80 to 150 km range over a slightly larger time window. Fig. 9 shows similar observed and modelled seismograms for more distant stations in the 200–300 km range. In both cases, the synthetic seismograms were generated using the method of Herrmann (1996) and a source depth of 14 km. The synthetics capture many of the features of the observations, for example, the modelled *P*- and *S*-waves at stations HBL2 and KEY2 are reasonable in terms of both arrival time and relative amplitudes between various phases. Goodness of fit begins to decrease with distance, which may be a consequence of lateral variability in structure. However, we conclude that the 14 km source depth provides a good overall match for the observed waveforms and qualitative evidence that the earthquake did occur at mid-crustal depth.

6. A comparison of aftershocks with main event

The Dudley mainshock was followed by two aftershocks that were also recorded on the BGS seismic network. The earthquakes occurred on 23 September at 03:32 and 24 September at 09:29, with magnitudes 2.7 ML and 1.2 ML, respectively. Accurate *P*-wave arrival times were identified on stations within 116 km from the epicentre location of the mainshock for the three events in order to resolve the relative location of the three events. Relative time differences between the stations were generally of the order of 0.1 s and did not provide any additional evidence on the relative locations

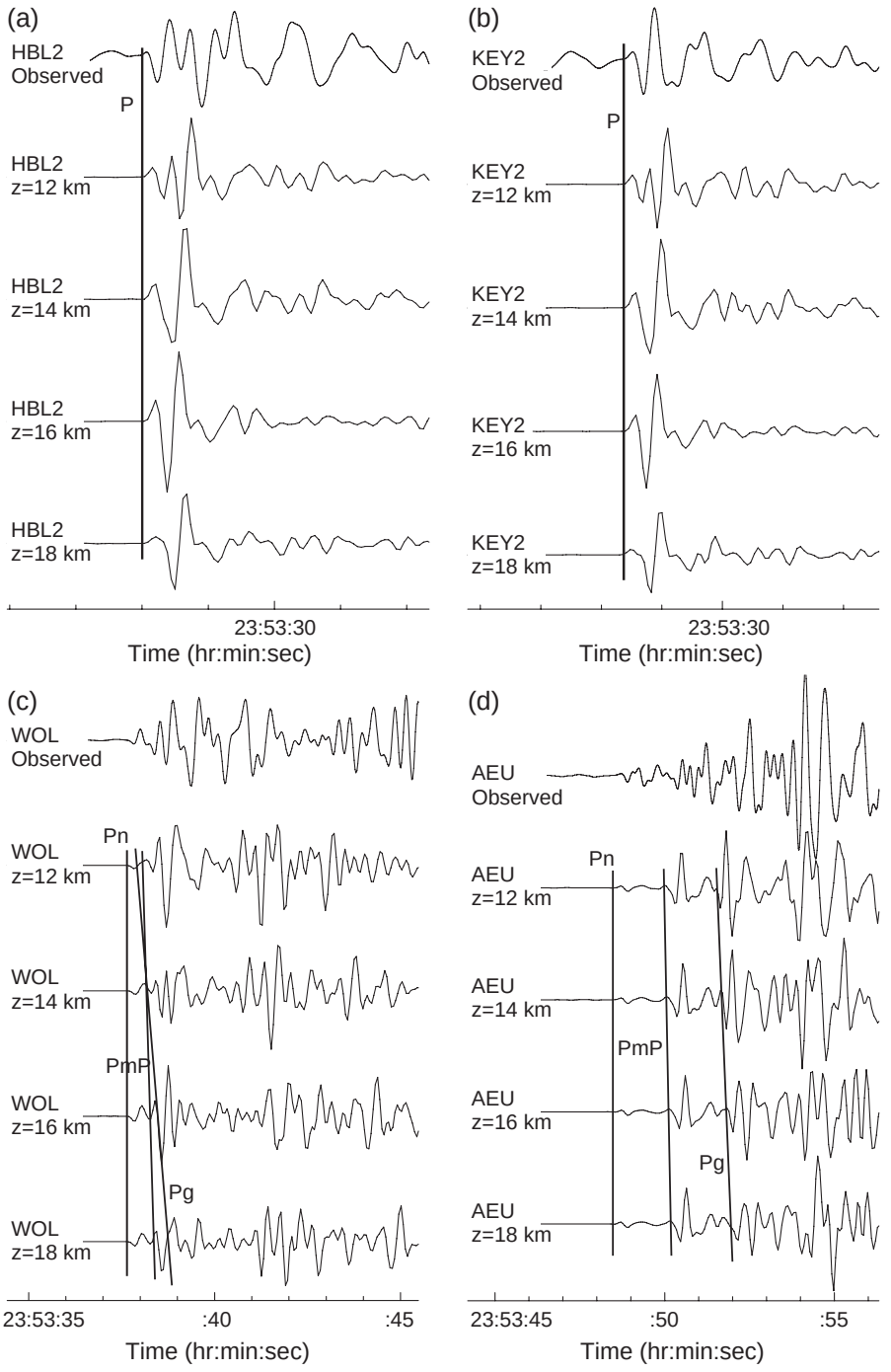

Fig. 7. Observed and modelled ground displacement seismograms for four source depths of 12, 14, 16 and 18 km at stations (a) HBL2, epicentral distance 80 km, (b) KEY2, epicentral distance 82 km, (c) WOL, epicentral distance 149 km, (d) AEU, epicentral distance 230 km. A band-pass filter of 1–4 Hz has been applied to the data.

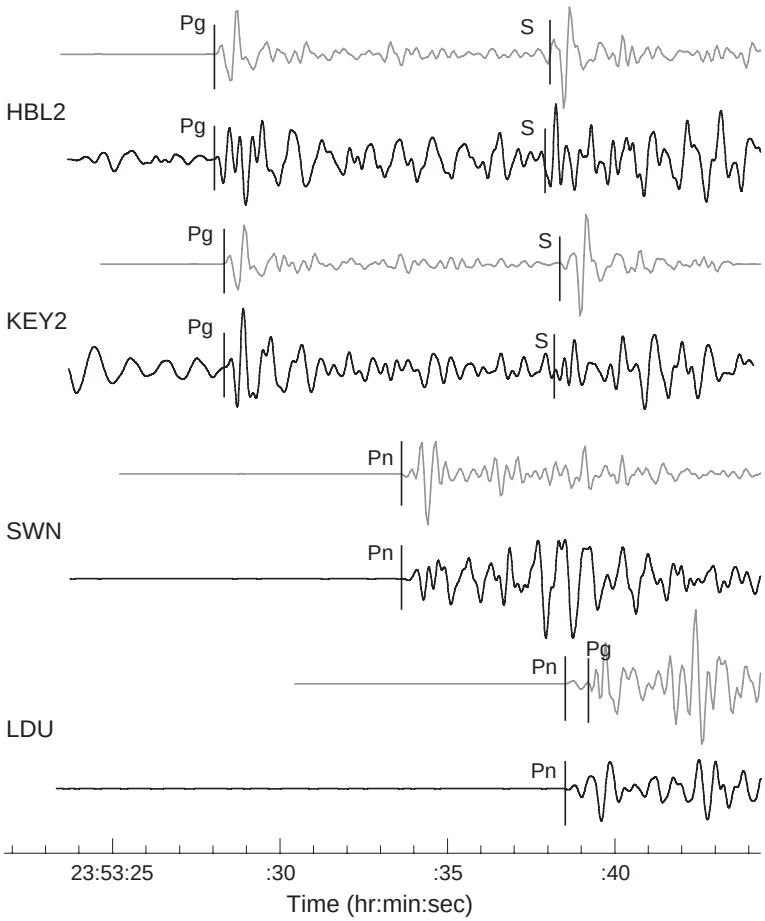

Fig. 8. Observed (black) and modelled (grey) ground displacement seismograms for stations HBL2 (80 km), KEY2 (82 km), SWN (115 km), LDU (148 km) and WOL (149 km). The synthetics were generated using a source depth of 14 km.

since the observed differences were of the same size as the error in phase reading. In a more formal approach, the three events were jointly located using the program VELEST (Kissling et al., 1994). The results (Table 2) show that the two aftershocks were located within the error ellipsoid (90% confidence) of the mainshock. However, the relative differences possibly reflect only the uncertainties in the phase identification.

Detailed inspection of waveforms from the first aftershock shows a small initial arrival that precedes the larger second arrival by 0.30 s (Fig. 10). The first (P1) and second waveform signals (P2) appear to be nearly identical and are separated by an offset that does not vary from station to station. This suggests that there were two events, the first and smaller event, possibly initiating the rupture, was followed by a larger event, which mostly contributed to the signal recorded as the first aftershock. Similar observations were made for earthquakes in California by Ellsworth and Beroza (1995), who interpreted this as rupture nucleation.

Comparison of signals from the mainshock and the first aftershock on a number of stations (Fig. 11) reveals a high degree of similarity, both with respect to phase arrival times as well as amplitude ratios between the various phases. The similarity in arrival times between the two events at a number of stations indicates that they are co-located. The match of amplitude ratios of seismic phases between events can be explained by a similar source mechanism. Unfortunately, the number of stations suited for

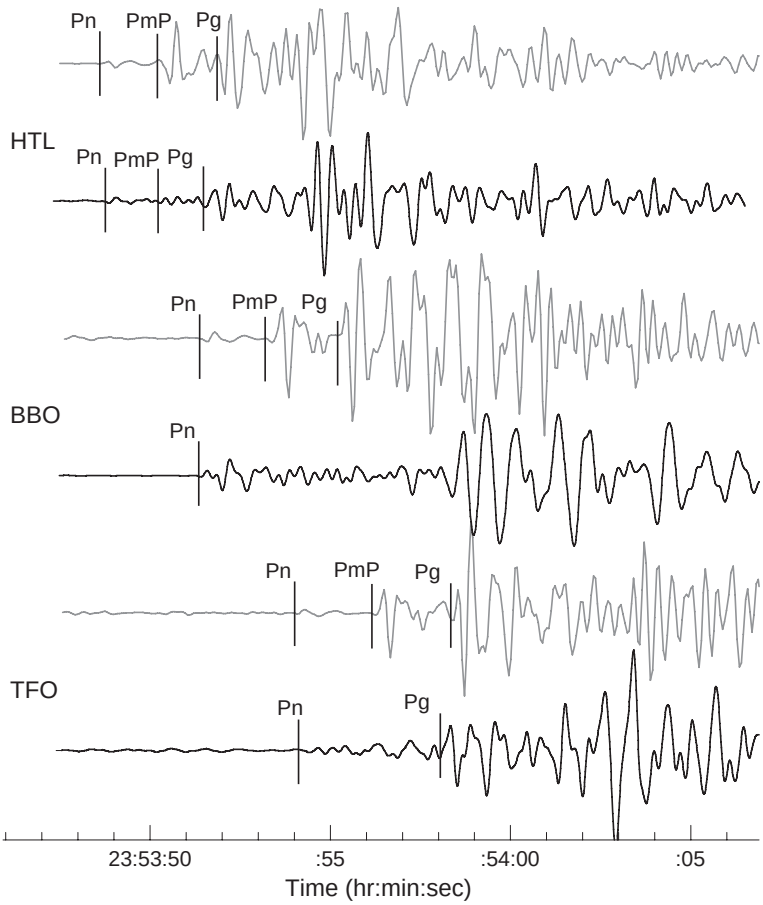

Fig. 9. Observed (black) and modelled (grey) ground displacement seismograms for stations AEU (230 km), HTL (234 km), BBO (256 km) and TFO (276 km). The synthetics were generated using a source depth of 14 km.

comparison of the main- and first aftershock is rather limited, since data for the mainshock at shorter distances on normal gain instruments are clipped. At the same time, since the aftershock is of much smaller size, the strong motion or low-gain instruments at shorter distances did not record the signals with sufficient amplitude for comparison, while at larger distances the signal to noise ratio was reduced compared to the larger mainshock. However, from the limited number of stations available, it seems likely that both mainshock and aftershock had a similar source mechanism.

Comparison of waveform signals between the two aftershocks from a number of stations also showed strong similarities (Fig. 12). It therefore seems likely that both events are very similar with respect to hypocentre location and mechanism. A perfect match between the two aftershocks cannot be expected due

Table 2
Results of joint hypocentre determination of the mainshock and its two aftershocks

Date	Origin time	Latitude	Longitude	Depth (km)	No. of stations	RMS (s)
2002/09/22	23:53:14.6	52.528	2.139	15.7	9	0.064
2002/09/23	03:32:15.9	52.526	2.145	13.1	9	0.055
2002/09/24	09:29:19.2	52.533	2.156	14.2	4	0.054

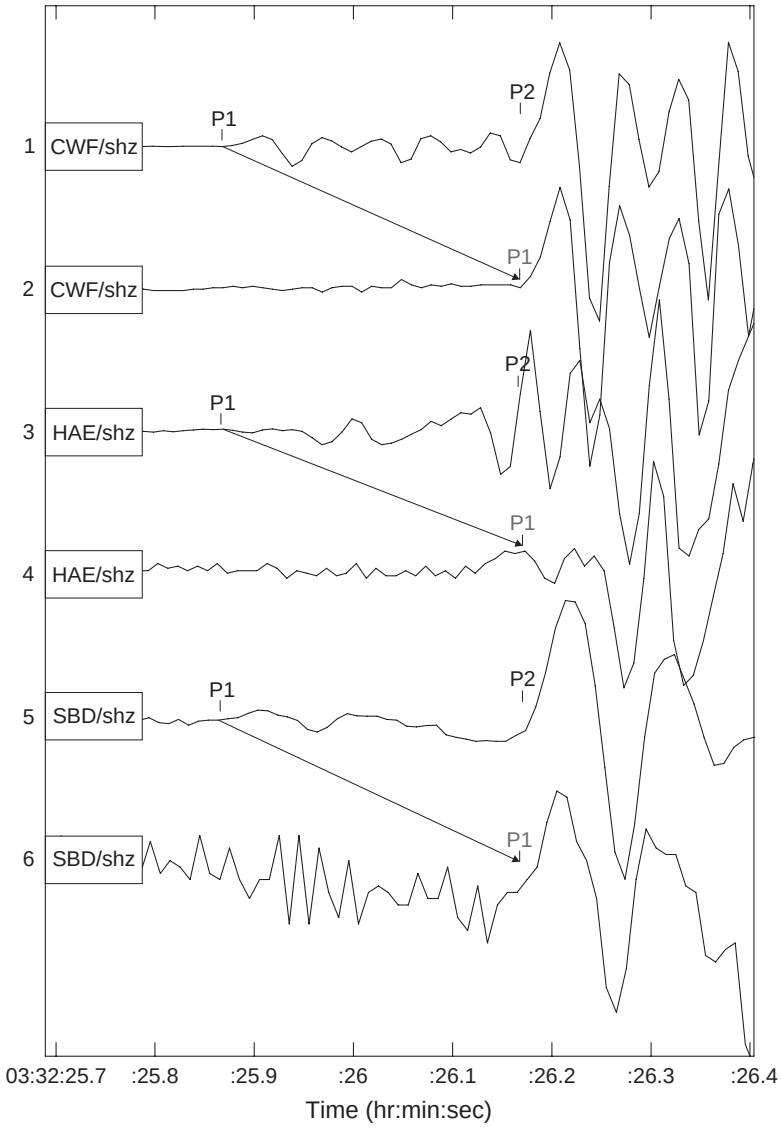

Fig. 10. Ground velocity seismograms from the first aftershock at 03:32 UTC on 23 September. The precursory signal has been aligned in time and scaled by a factor of 10 to the same amplitude as the larger arrival to show the similarity of the signals at the three stations CWF, HAE and SBD.

to the complexity of the first aftershock as it is preceded by a smaller event.

The source mechanism of the aftershocks could not be obtained directly due to the complexities of the first and the small size of the second, which did not allow the determination of a sufficient number of polarities. However, the comparison of waveform signals indicates that the three events probably had a similar or even identical mechanism. The few polarity readings that could be made for the first aftershock do not contradict this suggestion.

7. Peak ground motion

Fig. 13 shows the decay in observed peak vertical ground acceleration (PVGA) with hypocentral distance for the main shock and the largest aftershock.

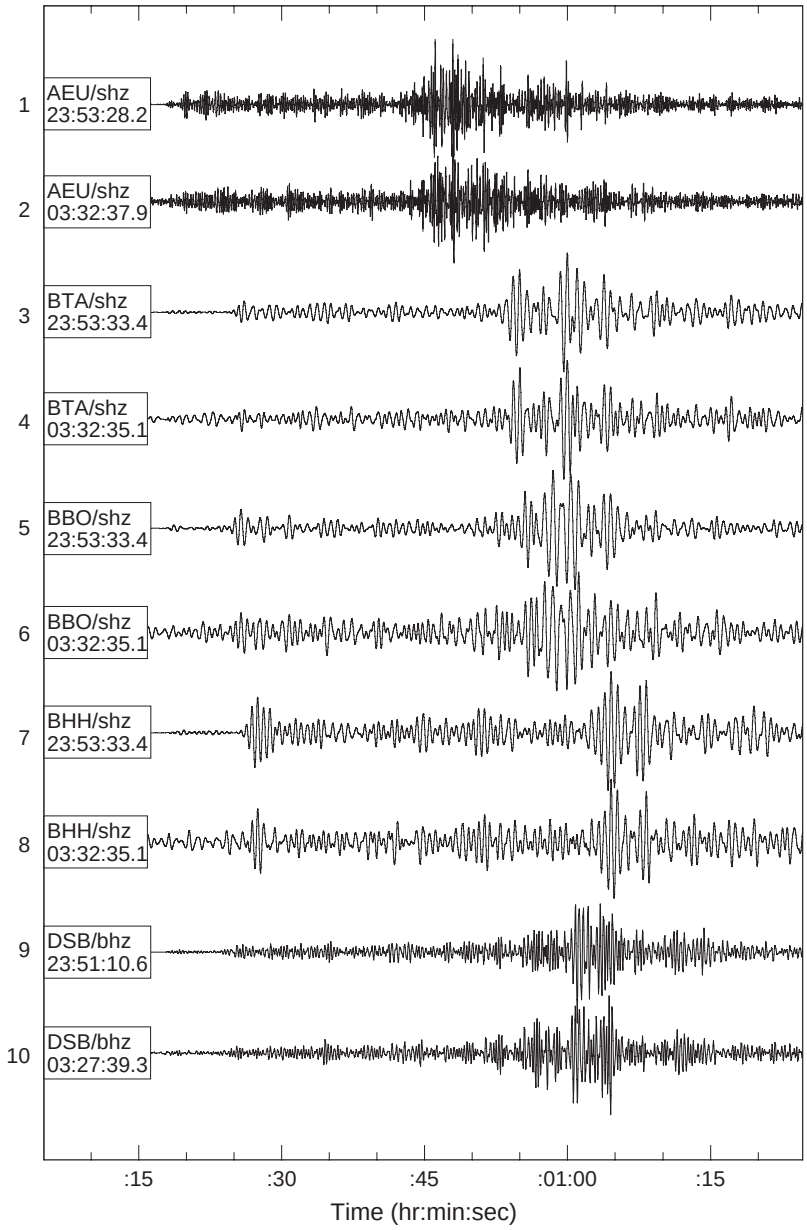

Fig. 11. A comparison of the waveforms from the mainshock and the first aftershock at 03:32 UTC on 23 September. All traces have been band-pass filtered: trace numbers 1, 2, 9 and 10 are filtered from 3 to 8 Hz; trace numbers 3 to 8 are filtered from 2 to 4 Hz.

Hypocentral distance, r_{hyp}, was calculated using a source depth of 14 km. Because deconvolving the instrument response amplifies noise outside the pass-band of the recording instrument, all signals were filtered between 1 and 25 Hz before measurements were made. PVGA decays exponentially from 15.3 cm/s^2 at station KEY2 (r_{hyp}=85 km) to 0.05 cm/s^2 at station JRS (r_{hyp}=371 km). KEY2 is the only station where the peak acceleration is observed in the *P*-wave. The general scatter in the observed peak ground motion values is primarily a result of variation in attenuation, both along the path and at the station.

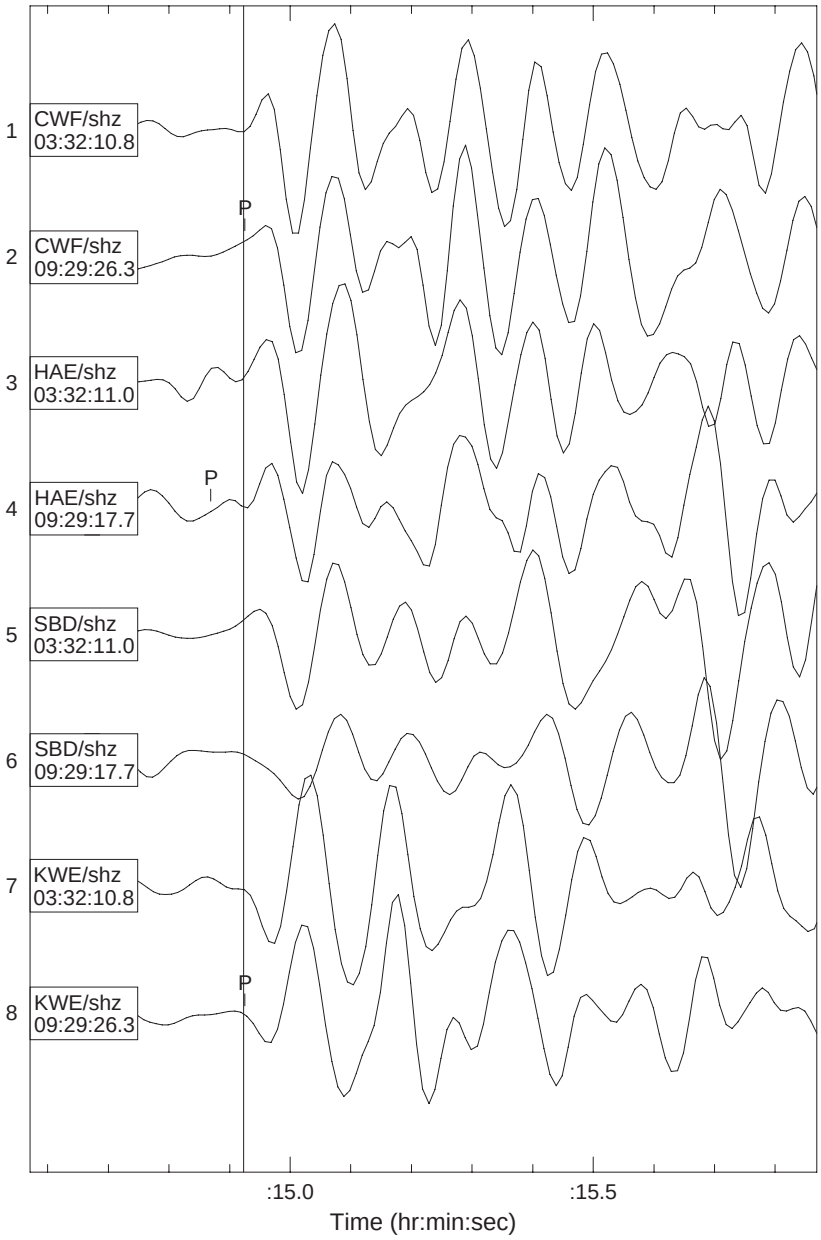

Fig. 12. A comparison of the ground velocity waveforms from the first aftershock at 03:32 UTC on 23 September and second aftershock at 09:29 UTC on 24 September at four stations CWF, HAE, SBD and KWE.

There are 47 observations of PVGA for the largest aftershock, recorded at distances between 64 km and 346 km from the epicentre (Fig. 13). These observations exhibit more scatter than for the mainshock, because the corner frequency is higher and the signal more sensitive to variations in the quality factor Q and the parameter κ describing near-surface attenuation.

Fig. 14 shows the observed peak horizontal ground acceleration (PHGA) for the mainshock. PHGA is defined as the maximum of the peak accelerations observed on the radial and transverse components.

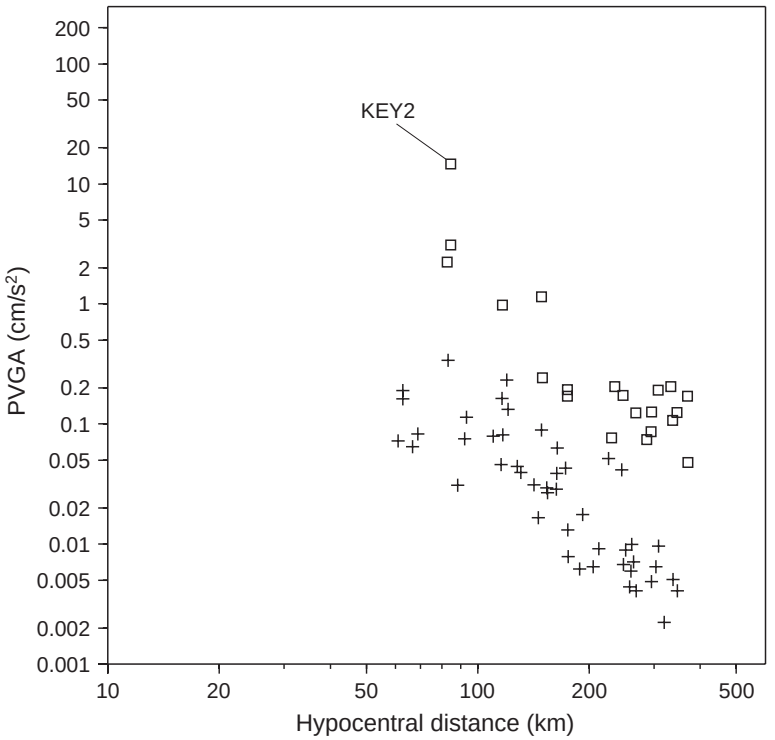

Fig. 13. The decay of vertical ground acceleration (PVGA) with hypocentral distance for the mainshock (squares) and the largest aftershock (crosses).

PHGA decays exponentially with distance from 15.6 cm/s^2 at KEY2 to 0.02 cm/s^2 at station MCD (r_{hyp}=568 km). Again the highest on-scale ground acceleration within the frequency band is observed in the *P*-wave at KEY2, 15.6 cm/s^2. However, the peak acceleration associated with the shear wave at this station is 6.3 cm/s^2, a value more consistent with the other observations. The average ratio of PHGA to PVGA is 1.71 ± 0.26. This is comparable to the ratio of 1.6 ± 0.6 found for firm soil and bedrock sites in Canada (Cassidy et al., 1997).

PHGA values predicted using the empirical relations derived by Ambraseys and Bommer (1991) and Toro et al. (1997), both of which have been considered applicable in the UK, are also shown in Fig. 14. Both these relations overestimate the observed PHGA. However, to make this comparison, these relations have been extended below the magnitude range for which they have been validated. As a result, the apparent overestimation of PHGA may not actually be due to differences in attenuation, but rather a change in magnitude scaling of PGA for smaller earthquakes, as observed by Douglas (2003).

8. Predicting peak ground acceleration using random vibration theory

An attenuation relation that is specific to the UK has yet to be developed due to the lack of data, particularly from larger earthquakes. However, in low seismicity regions, the stochastic method (Boore, 1983) can be used to synthesise ground motion datasets from which attenuation relations can be derived. Such an approach has proved effective in areas such as eastern North America (Toro et al., 1997).

Here, PHGA is simulated using the results of random vibration theory (RVT) (Vanmarcke and Lai, 1980). Unlike Boore's stochastic method, which simulates the acceleration time history to determine PHGA, RVT permits PHGA to be calculated directly from the theoretical acceleration spectrum. Boore

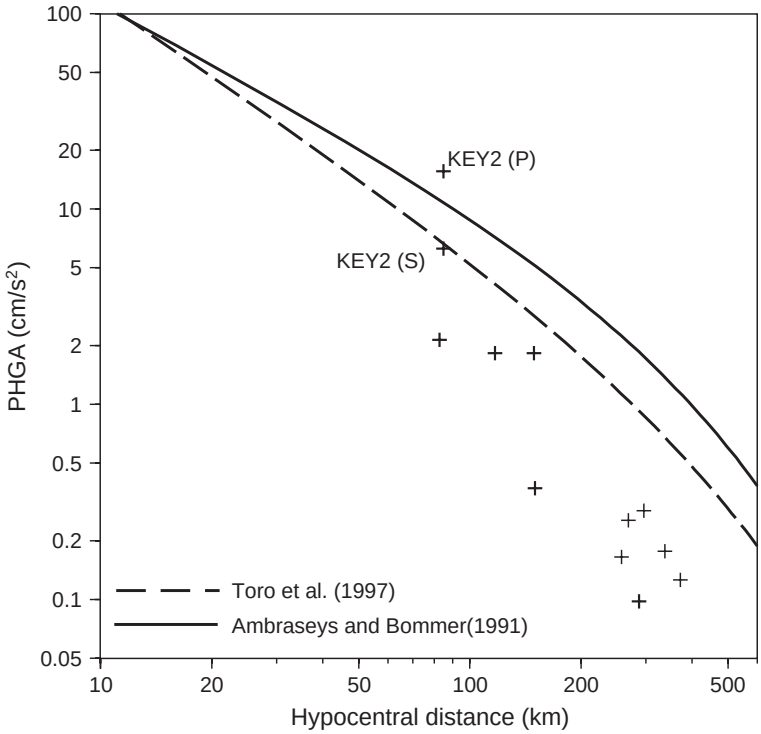

Fig. 14. Observed values of peak horizontal ground acceleration (PHGA) for the mainshock from strong motion (triangles), short period (circles) and broadband instruments (squares), compared with the values predicted by (Ambraseys and Bommer, 1991) (solid line) and (Toro et al., 1997) (dashed line).

(1983) shows that the results obtained using the RVT approach are comparable to the peak motions estimated from simulated time series.

Provided that the seismic moment M_0 and stress drop $\Delta\sigma$ are known, PHGA can be calculated from the theoretical acceleration spectrum using the results of RVT (Vanmarcke and Lai, 1980). Using the first (mean), second (variance) and fourth statistical moments of the energy density spectrum, the spectral bandwidth, RMS acceleration (A_{RMS}) and predominant frequency may be found. Maximum acceleration can then be determined from A_{RMS} and the expected number of acceleration extrema in a specified time interval (assuming a stationary time series with uncorrelated peaks).

PHGA is estimated over a range of distances ($5 < r_{\mathrm{hyp}} < 600$ km). Hypocentral distance is used because the extent of the rupture is small ($R \simeq 1$ km), and using epicentral distance or the Joyner-Boore distance may cause ground motion to be overestimated, particularly in the near-field.

Seismic moment, M_0, and corner frequency, f_c, were determined from the vertical displacement spectrum of the L_g-wave using the automated converging grid-search method of Ottemoller and Haskov (2003). The portion of the seismogram used to calculate the spectrum was defined by the group velocity window 3.0–3.6 km/s.

The closest unsaturated records for the mainshock and the largest aftershock are from epicentral distances of 80 km and 64 km, respectively. The initial data set for each earthquake included all on-scale records where L_g was clearly observed. Those records, which did not meet the prescribed signal-to-noise criteria used by the program over a wide enough range of frequencies for f_c to be determined reliably, or those where the spectrum deviated significantly from the expected two-piece spectral model, were removed from the final data set used to calculate the average source parameters.

Observed spectra were corrected for geometrical spreading, path and near-surface attenuation, source

radiation and free-surface effects. A new relation for Q (the quality factor) was provided by Sargeant et al. (2004): $Q=402(1+(f/7.1)^{1.76})$. Near-surface attenuation was assumed to be of the form $-e^{\pi\kappa f}$ given by Anderson and Hough (1984), with $\kappa=0.02$ s assumed at all stations.

The results of the spectral analysis for the mainshock and the largest aftershock respectively are given in Tables 3 and 4. The zero-level frequency of the displacement amplitude spectra, Ω_0, is well-constrained for both earthquakes: 3.7 ± 0.2 for the mainshock and 2.1 ± 0.2 for the aftershock. Corner frequency is more uncertain due to its trade-off with the near-surface attenuation at each station, which is unknown. For the mainshock $f_c=1.98\pm0.46$ Hz and 8.99 ± 2.02 Hz for the aftershock. With the combined errors on Ω_0 and f_c, average stress drops are poorly constrained but are both around 30 bars. This corresponds to rupture radii of less than 1 km and less than 0.5 km for the mainshock and aftershock, respectively. The average moment magnitude of the mainshock is 4.1 ± 0.12 and agrees with the estimate published by the Swiss Seismological Service (4.3 M_w). For the aftershock, we found $M_w=2.76\pm0.15$.

Table 3
Source parameters for the mainshock (4.7 ML) determined automatically from vertical L_g-wave spectra1

Station	R (km)	Log M_0	$\Delta\sigma$ (bars)	Ω_0	f_c (Hz)	M_w	Azimuth
XDE	238	15.2	38.4	3.8	2.27	4.1	338
EAU	241	15.4	20.7	3.9	1.57	4.2	347
BBO	257	15.2	39.9	3.8	2.29	4.1	344
BDL	259	15.5	58.7	4.1	2.10	4.2	348
BTA	267	15.5	42.2	4.1	1.85	4.3	353
BHH	294	15.2	59.9	3.8	2.50	4.1	346
BBH	295	15.4	39.3	4.0	1.91	4.2	350
GMM	316	14.9	43.1	3.4	2.96	3.9	307
ESK	318	14.9	11.4	3.4	1.90	3.9	345
ESY	379	15.3	19.4	3.8	1.64	4.1	355
PCA	379	15.1	18.6	3.6	1.84	4.0	339
EDI	384	15.3	16.5	3.8	1.60	4.1	350
PCO	405	15.4	9.3	3.8	1.23	4.2	342
PMS	406	15.5	10.5	3.9	1.17	4.3	335
EAB	431	15.2	17.7	3.6	1.75	4.1	341
EDU	451	15.3	21.7	3.7	1.71	4.1	353
EDR	489	15.3	64.0	3.7	2.48	4.1	357
MDO	564	14.9	39.4	3.3	2.80	3.9	346
MCD	567	15.4	27.3	3.8	1.73	4.2	353
MVH	614	15.2	32.9	3.5	2.19	4.0	348
RRR	636	15.0	20.6	3.4	2.06	4.0	339
Average		15.24	31.02	3.72	1.98	4.10	
σ		0.19	16.59	0.23	0.46	0.12	

Table 4
Source parameters for the largest aftershock (2.7 ML) determined automatically from vertical L_g-wave spectra

Station	R (km)	Log M_0	$\Delta\sigma$ (bars)	Ω_0	f_c (Hz)	M_w	Azimuth
SSW	64	12.9	25.0	1.9	11.51	2.5	161
KTG	119	13.6	89.5	2.4	10.23	3.0	100
WFB	129	13.2	31.1	2.0	9.95	2.7	278
WPM	144	13.3	5.9	2.1	5.17	2.8	305
YLL	152	13.2	17.4	2.0	8.12	2.7	297
YRE	162	13.3	24.5	2.0	8.55	2.8	289
YRH	171	13.2	31.8	2.0	9.39	2.8	282
Average		13.24	32.17	2.06	8.99	2.76	
σ		0.21	26.79	0.16	2.02	0.15	

These results provided the necessary input for estimating peak ground acceleration. In Figs. 15 and 16, observed PHGA from the two earthquakes is shown along with the theoretical values for four scenarios: the average source model with $\kappa=0.01$ and 0.02 s and three standard deviations (σ) above the average source model, again with $\kappa=0.01$ and 0.02 s. Using $\kappa=0.02$ s, the estimated peak accelerations from the average models define the lower bound on the PHGA observations from both events. Three σ above the mean, the theoretical values define the upper bound on PHGA for the aftershock but tend to underestimate the majority of observations for the mainshock.

Assuming that the model is valid in the near-field, PHGA at the epicentres was estimated using $\kappa=0.01$ s. At the mainshock epicentre, PHGA is estimated to be 0.012 g for the average source model and 0.035 g at three standard deviations above the average model. Estimated PHGA at the epicentre of the aftershock is 0.0034 g (and 0.014 g at three standard deviations above the mean). Without any near-field observations of ground acceleration or site effect information, these values should be regarded as only rough approximations of PHGA at the epicentre.

9. Discussion

Instrumental data have been used to determine a hypocentre and source mechanism for the Dudley earthquake. The earthquake epicentre appears to be well constrained, with good azimuthal coverage,

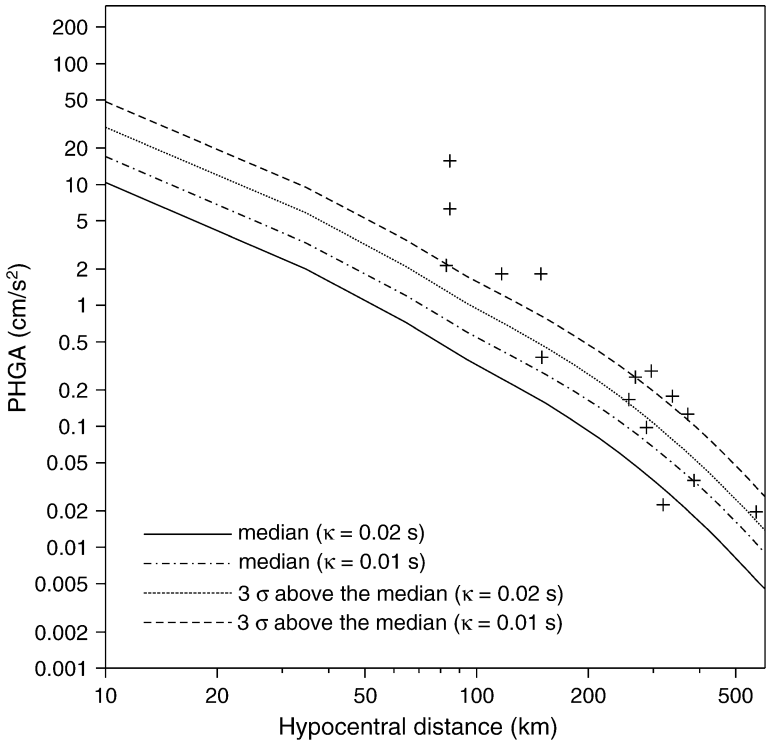

Fig. 15. Comparison of observed PHGA for the mainshock with theoretical values using RVT. Crosses show the observed data. The solid black line shows PHGA calculated using average $\Delta\sigma$ and M_w from Table 3 and $\kappa = 0.02$. The dotted line shows a more conservative estimate of PHGA calculated using the standard deviation on $\Delta\sigma$ and M_w.

although the closest station is 58 km distant. Focal depth is less well constrained, though the distribution of RMS errors with depth shows a clear minimum at 14 km. However, both depth and mechanism depend on the seismic velocity model used to locate the earthquake and determine source takeoff angles, which can add to the uncertainty in both. In this case, the velocity model is rather poorly known. Most of the published information on seismic velocity structure in the UK has been obtained from large-scale seismic refraction and wide-angle reflection surveys carried out by various institutes (Booth, 2001) and the 1-D models of seismic velocity as a function of depth used by BGS for earthquake location in the UK are derived from these studies. However, few refraction profiles have been carried out in central and southern England and the 1-D model derived for the Midland valley of Scotland has commonly been applied to this region. This model divides the crust into three main units, typically observed across the UK: a sedimentary overburden, a crystalline upper crust of deformed metamorphic and igneous rocks, and a lower crust. Previous results suggest that this is a reasonable approximation with earthquakes and other seismic events generally being located within a few kilometres of the area of peak intensity. However, no calibration studies have been undertaken for events in this region. Table 5 shows the dependence of hypocentre depth on the Moho depth for the Dudley earthquake. The source depth increases from 8 to 15 km as the depth to the Moho and crustal thickness increases. The overall crustal thickness used in the 1-D model is 34 km. Chadwick and Pharaoh (1998) find a depth for the seismic reflection Moho in the Midlands of 32–34 km, though this is poorly constrained, and Tomlinson et al. (2003) find a crustal thickness of 34–36 km from teleseismic receiver functions determined at three-component stations within 62–80 km of the Dudley epicentre.

Two independent methods of determining the earthquake source mechanism give very similar solutions, except for small variations in the directions

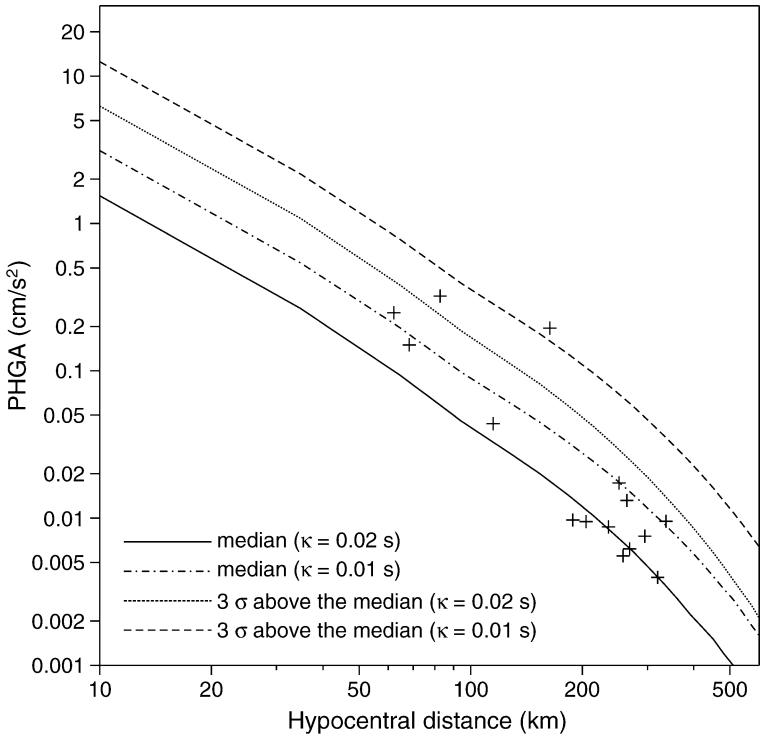

Fig. 16. Comparison of observed and theoretical PHGA for the first aftershock. Crosses show the observed data. The solid black line shows PHGA calculated using average $\Delta\sigma$ and M_w from Table 4. The dotted line shows a more conservative estimate of PHGA calculated using the standard deviation on $\Delta\sigma$ and M_w.

of dip and slip. The focal mechanism determined using first motion polarities is relatively insensitive to changes in focal depth and within the depth error of 3.7 km the mechanism remains unchanged, suggesting that this solution does not have a critical dependence on the velocity model and is reasonably robust. The moment tensor inversion showed that the event cannot be shallower than about 9 km. However, solutions of up to about 30 km would still match the observed data (Braunmiller, 2003, pers. comm.). The calculated direction of maximum compressive stress also shows good agreement with the expected stress regime from a regional tectonic model dominated by northwest compression from the Mid-Atlantic Ridge, and with the best-fitting stress tensor given by inversion of UK earthquake focal mechanisms.

Table 5
Dependency of source depth with Moho depth

Moho depth (km)	Source depth (km)	RMS
30	8.1	0.31
31	10.0	0.31
32	10.6	0.31
33	11.8	0.31
34	12.7	0.33
35	14.4	0.34
36	15.2	0.37

Waveform modelling provides further support for a focal depth of 14 km, but again there is a strong dependence on the velocity model used to generate the synthetics. Lateral variation in structure is likely to cause significant variations in the observed seismograms both with distance and azimuth. Therefore, waveform modelling has to be used with caution as a quantitative tool to constrain source depth by modelling high frequency data.

The earthquake epicentre lies in a major zone of faulting associated with the Western Boundary Fault of the South Staffordshire Coalfield, an important basin-controlling normal fault with significant syndepositional throw. It seems likely that the fault, or faults, associated with this zone could have caused the

earthquake. The surface trace of the Western Boundary Fault passes to the west of Dudley and to the east of Stourbridge along a southerly or south-easterly trend (Fig. 3) and the fault throws down Triassic rocks to the west against older (Upper Carboniferous) rocks of the South Staffordshire Coalfield to the east. The epicentre was estimated at a depth of 14 km and about 1 km to the west of the Western Boundary Fault. The horizontal error in epicentre determination is 1–3 km, which means that any of several faults could have been the source of the event. The majority of the larger faults trend NE–SW, which may indicate that the north–south nodal plane is more likely to be the fault plane of the earthquake. The westward dip of the Western Boundary Fault shows better agreement with the moment tensor solution than the solution from first motion polarities; however, it is unknown how the faults continue at depth. The mid-crustal depth of the earthquake implies either that the fault zone extends from the surface to significant depths, or that the earthquake occurred on an older fault, deeper in the crust, that has a similar orientation.

The similarity of the waveforms between the mainshock and the aftershocks suggests that they all occurred within a small source volume, of the order of a few hundred m. In addition, the complex nature of the waveforms for the first and largest aftershock suggests that a two-stage rupture may have taken place, with a smaller rupture initiating further slip possibly along the same fault. The observed nucleation phase lasted for 0.30 s, which is significantly shorter than observed in California by Ellsworth and Beroza (1995). The difference is possibly explained by the dissimilarity in tectonic setting.

The average moment magnitude of 4.1 M_w, determined from the source spectra, is in keeping with the value of 4.3 M_w obtained by the moment tensor inversion of the Swiss Seismological Service. The Brune stress drop parameter, $\Delta\sigma$, has a large uncertainty associated with it, reflecting station-to-station variability of the corner frequency measurement. This variability could to some extent result from the assumed value for the near-surface attenuation parameter, κ, of 0.02 at all stations. Ideally, in studies of this type, datasets should be restricted to records from stations sited on hard rock, where κ is likely to be low and the assumption of a single value is appropriate. However, the wide distribution of drift and sedimentary rock in the UK makes this restriction unworkable. Assuming one κ value for the whole dataset makes it possible to find values for f_c and Ω_0 which fit the data well, but introduces greater uncertainty into the estimate of the stress parameter.

Using the stochastic method, it is possible to achieve a reasonably good fit between the observed and theoretical PHGA values for the Dudley mainshock and aftershock using a simple attenuation model. For future studies in the UK, it is likely that the quality of the fit could be further improved if the dataset could be restricted to records from stations sited on hard rock were included. However, with the lack of PHGA data in the UK, it would be preferable for κ to be reliably defined at each station rather than further reducing the size of the dataset.

10. Conclusions

- The source depth, constrained by waveform modelling, shows that the earthquake occurred in the mid-crust.
- The source mechanism suggests strike-slip faulting along a near-vertical fault-plane that strikes north–south. This observation is in agreement with both the surface expressions of faulting in the area and also with the expected regional stress tensor dominated by northwest compression from the Mid-Ocean Ridge.
- It seems likely that the earthquake can be associated with the Western Boundary Fault of the South Staffordshire Coalfield, a significant fault in the region.
- The mainshock and the aftershocks all occurred within a small source volume, of the order of a few hundred metres in extent and had similar source mechanisms.
- The rupture for the largest aftershock probably comprised two stages with a smaller rupture initiating further slip. A precursory phase was not observed for the mainshock.
- The observed peak ground acceleration is considerably less than that predicted by empirical relations which are currently used in the UK. A better match for the observed ground motions is achieved using a stochastic approach to model both the mainshock and the first aftershock.

Acknowledgements

The authors thank Jochen Braunmiller of the Swiss Seismological Service for providing the moment tensor solution and discussions on the uncertainties. Additional data used to locate the earthquake and determine a fault plane solution was provided by Keele University, AWE Blacknest (station WOL), IRIS/IDA (station ESK) and GEOFON (station DSB). Project IDA is a global network of broadband and very long period seismometers operated by the Institute of Geophysics and Planetary Physics, Scripps Institution of Oceanography, University of California, San Diego. The GEOFON network is funded and operated by GFZ Potsdam, Germany, in cooperation with almost 50 institutions worldwide. Julian Bukits assisted with diagrams. David Booth and Alice Walker are also thanked for their comments and suggestions. This work is published with the permission of the Executive Director of the British Geological Survey (NERC).

References

Ambraseys, N., Bommer, J., 1991. The attenuation of ground acceleration in Europe. Earthq. Eng. Struct. Dyn. 13, 307–320.

Anderson, J., Hough, S., 1984. A model for the shape of the Fourier amplitude spectrum of acceleration at high frequencies. Bull. Seismol. Soc. Am. 74, 1969–1993.

Assumpção, M., Bamford, D., 1978. LISPB V. Studies of crustal shear waves. Geophys. J. R. Astron. Soc. 54, 61–73.

Bamford, D., Nunn, K., Prodehl, C., Jacob, B., 1978. LISPB-IV. Crustal structure of Northern Britain. Geophys. J. R. Astron. Soc. 54, 43–60.

Baptie, B., 2002. The state of stress in the UK from observations of local seismicity. European Seismological Commission, XXVIII General Assembly, Genoa.

Bernardi, F., Braunmiller, J., Kradolfer, U., Giardini, D., 2002. Fully automated regional moment tensor inversion in the European Mediterranean area. European Seismological Commission, XXVIII General Assembly, p. 215.

Boore, D., 1983. Stochastic simulation of high-frequency ground motions based on seismological models of radiated spectra. Bull. Seismol. Soc. Am. 73, 1865–1894.

Booth, D., 2001. Review of velocity structure in the UK and adjacent areas. Technical Report CR/01/79, British Geological Survey.

Burton, P., Musson, R., Neilson, G., 1984. Macroseismic report on historical British earthquakes: IV. Lancashire and Yorkshire. Global Seismology Report vol. 219. British Geological Survey.

Cassidy, J., Rogers, G., Wiechert, D., 1997. Soil response on the Fraser Delta to the MW=5.1 Duvall, Washington, earthquake. Bull. Seismol. Soc. Am. 87 (5), 1354–1362.

Chadwick, R., Pharaoh, T., 1998. The seismic reflection Moho beneath the United Kingdom and adjacent areas. Tectonophysics 299, 255–279.

Douglas, J., 2003. A note on the use of strong motion records from small magnitude earthquakes for empirical ground motion estimation: Skopje Earthquake—40 years of European Earthquake Engineering (SE40EEE), Skopje, Macedonia.

Ellsworth, W., Beroza, G., 1995. Seismic evidence for an earthquake nucleation phase. Science 268, 851–855.

Herrmann, R., 1996. Computer Programs in Seismology. Saint Louis University.

Kissling, E., Ellsworth, W., Eberhart-Phillips, D., Kradolfer, U., 1994. Initial reference model in local earthquake tomography. J. Geophys. Res. 99 (19), 19635–19646.

Lienert, B., Berg, E., Frazer, L., 1988. HYPOCENTER, an earthquake location method using centered, scaled and adaptively least squares. Bull. Seismol. Soc. Am. 76, 771–783.

Main, I., Irving, D., Musson, R., Reading, A., 1999. Constraints on the frequency magnitude relation and maximum magnitudes in the UK from observed seismicity and glacio-isostatic recovery rates. Geophys. J. Int. 137, 535–550.

Musson, R., 1994. A catalogue of British earthquakes. Technical Report WL/94/04, British Geological Survey.

Musson, R., Neilson, G., Burton, P., 1984. Macroseismic report on historical British earthquakes: XII. North Wales and Irish Sea. Global Seismology Report vol. 28. British Geological Survey.

Nabelek, J., Xia, G., 1995. Moment tensor analysis using regional data: application to the 25 March, 1993, Scotts Mills, Oregon, earthquake. Geophys. Res. Lett. 22, 13–16.

Neilson, G., Musson, R., Burton, P., 1986. Macroseismic report on historical British earthquakes XI: 1931 June 7 North Sea. Global Seismology Report vol. 280. British Geological Survey.

Ottemoller, L., Haskov, J., 2003. Moment magnitude determination for local and regional earthquakes based on source spectra. Bull. Seismol. Soc. Am. 93 (1), 321–326.

Pharaoh, T., Molyneux, S., Merriman, R., Lee, M., Verniers, J., 1993. The Caledonides of the Anglo-Brabant Massif reviewed. Geol. Mag. 130 (5), 561–562.

Powell, J., Glover, B., Waters, C.N., 1992. A geological background for planning and development in the Black Country. Technical Report WA/92/33, British Geological Survey.

Ritchie, M., Musson, R., Woodcock, N., 1990. The Bishop's Castle earthquake of 2 April 1990. Terra Nova 2, 390–400.

Sargeant, S., Ottemoller, L., Musson, R., 2004. Lg wave attenuation in the UK. European Seismological Commission XXIX General Assembly, Potsdam.

Simpson, B., 2002. A Bulletin of British Earthquakes 2002. Technical Report WL/02/01, British Geological Survey.

Snoke, J., Munsey, J., Teague, A., Bollinger, G., 1984. A program for focal mechanism determination by combined use of polarity and SV-P amplitude ratio data. Earthq. Notes 55, 3–15.

Tomlinson, J., Denton, P., Maguire, P., Evans, J., 2003. UK crustal structure close to the Iapetus Suture: a receiver function perspective. Geophys. J. Int. 154, 659–665.

Toro, G., Abrahamson, N., Schneider, J., 1997. Model of strong ground motions from earthquakes in Central and Eastern North America: best estimates and uncertainties. Seismol. Res. Lett. 68 (1), 41–73.

Vanmarcke, E., Lai, S.-S., 1980. Strong motion duration and RMS amplitude of earthquake records. Bull. Seismol. Soc. Am. 70 (4), 1293–1307.